

DAReN: A Collaborative Approach Towards Reasoning And Disentangling

Prithish Sahu, Vladimir Pavlovic
Rutgers University
Piscataway, NJ 08554

Computational learning approaches to solving visual reasoning tests, such as Raven’s Progressive Matrices (RPM), critically depend on the ability of the computational approach to identify the visual concepts used in the test (i.e., the representation) as well as the latent rules based on those concepts (i.e., the reasoning). However, learning of representation and reasoning is a challenging and ill-posed task, often approached in a stage-wise manner (first representation, then reasoning). In this work, we propose an end-to-end joint representation-reasoning learning framework, which leverages a weak form of inductive bias to improve both tasks together. Specifically, we propose a general generative graphical model for RPMs, *GM-RPM*, and apply it to solve the reasoning test. We accomplish this using a novel learning framework **Disentangling based Abstract Reasoning Network (DAReN)** based on the principles of *GM-RPM*. We perform an empirical evaluation of DAReN over several benchmark datasets. DAReN shows consistent improvement over state-of-the-art (SOTA) models on both the reasoning and the disentanglement tasks. This demonstrates the strong correlation between disentangled latent representation and the ability to solve abstract visual reasoning tasks.

1 Introduction

Raven’s Progressive Matrices (RPM) (Raven 1941, 1936; Raven and Court 1998) is a widely acknowledged metric in the research community to test the cognitive skills of humans. The purpose of RPM is primarily to assess a person’s capacity to perform comparisons, reason by analogy, logical thinking processes. Thus RPM task is considered to have the highest “g-loading” and plays a central role among most cognitive tests (Klein, Raven, and Fodor 2018).

Vision community has often employed Raven’s test to evaluate the reasoning skills of an AI model (Carpenter, Just, and Shell 1990; Hoshen and Werman 2017; Little, Lewandowsky, and Griffiths 2012; Lovett and Forbus 2017; Lovett, Forbus, and Usher 2010; Lovett et al. 2009). These tests are presented as a matrix, where each cell contains visual geometric design except the last, which is kept empty (Figure 1). The AI model is designed to pick the best-fit images from a provided list of 6 to 8 choices. To correctly answer, the model has to deduce the abstract relationship between the visual features such as shape, position, color, size,

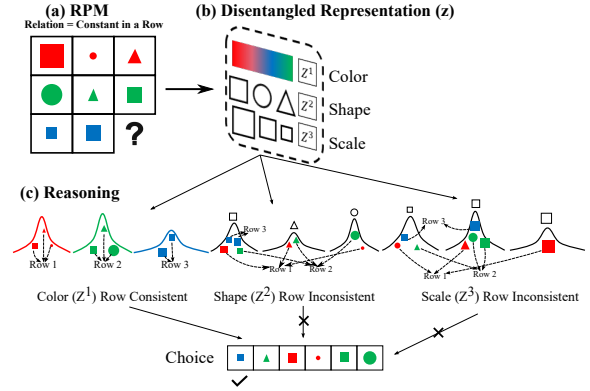


Figure 1: **a:** A sample instance of the RPM with missing bottom right image. **b.** The independent underlying generative factors of the images in RPM. **c.** Reasoning using the latent factors: A value at z^i is represented by a gaussian. The relation constant in a row is true at z^1 representing color while the other two factors are inconsistent in a row. The blue colored image from choice is the correct answer as it matches relation constant in a row for the last row.

and the underlying relationship that is applied on them in the matrix. These relationships were first proposed by (Carpenter, Just, and Shell 1990) that are constant in a row or column, quantitative pairwise progression, figure addition or subtraction, distribution of three values and distribution of two values. The visual IQ score of the model obtained from solving abstract reasoning tasks can provide ground to compare AI against human intelligence.

Please refer to Figure 1 for a demo example of RPM prepared by using the relation constant in a row. Initial stages of research employed computation models that depended on handcrafted heuristics rules on propositions formed from visual inputs to solve RPM (Carpenter, Just, and Shell 1990; Bringsjord and Schimanski 2003; Lovett, Forbus, and Usher 2007). Recent approaches use visual representation from neural networks to solve RPM (Hoshen and Werman 2017; Barrett et al. 2018; Zhang et al. 2019; van Steenkiste et al. 2019). The latest proposed model by (Barrett et al. 2018) known as Wild Relation Network (WReN) is the current state of the art neural network based on Relation Net-

work (Santoro et al. 2017) for Raven’s test. While WReN outperforms other reasoning based models on datasets such as PGM (Barrett et al. 2018), Raven (Zhang et al. 2019), the performance is still sub optimal compared to humans.

These setbacks to the model performance is caused due to the lack of effective and task-appropriate visual representation. The model’s during the training should separate apart the key attributes needed for reasoning. These key attributes aka disentangled representations (Bengio, Courville, and Vincent 2013; Ridgeway 2016) breaks down the visual features to its independent generative factors, i.e., to factors that can be used to generate the full spectrum of variations in the ambient data. We argue that a better disentangled model is essential for better reasoning ability of machines. In a recent study (Locatello et al. 2019a) via impossibility theorem has shown the limitation of learning disentanglement independently. The impossibility theorem states without the presence of any form of inductive bias, learning disentangled factors is impossible. Since collecting label information of the generative factors is challenging and almost impossible in real world datasets, previous works have focused on some form of semi-supervised or weakly-supervised methods such as observing a subset of ground truth factors (Kingma et al. 2014), using paired images that share values for a subset of factors (Bouchacourt, Tomioka, and Nowozin 2018) or knowing the rank of subset of factors for a pair of images (Wang et al. 2014) to improve disentanglement. In our work, we improve upon the model’s reasoning ability by using the inductive reasoning present in the spatial features. This underlying reasoning induces weak supervision that helps improve disentanglement hence leading to better reasoning.

Our work considers the upside of jointly learning disentangled representation and learning to reason (critical thinking). First, unlike above proposed models, i.e (working in a staged process either to improve disentangling or improve downstream accuracy), we work on the weakness of both components and propose a novel way to optimize both in single end-to-end trained model. We demonstrate the benefits of the interaction between the representation learning and reasoning ability.

Our motivation behind using the same evaluation procedure by (van Steenkiste et al. 2019) is as follows: 1) the strong visual presence 2) information of the generative factors help in demonstrating the model efficacy on both reasoning accuracy and disentanglement (strong correlation) 3) possibility of comparing the disentangled results with state-of-the-art SOTA disentangling results.

Our contributions are summarized as follows:

- We propose a general generative graphical model for RPM, GM-RPM, which will form the essential basis for inductive bias in joint learning for representation + reasoning.
- Building upon GM-RPM, we propose a novel learning framework named **Disentangling based Abstract textbf-Reasoning Network (DAReN)** composed of two primary components— disentanglement network, and reasoning network. It learns to disentangle factors and uses the rep-

resentation to detect both the underlying relationship and the object property used for the relation.

- We show that DAReN outperforms all SOTA baseline models across reasoning and disentanglement metrics, demonstrating that reasoning and disentangled representations are tightly related; learning both in unison can effectively improve the downstream reasoning task.

2 Related Works

Visual Reasoning. Earlier works on abstract visual reasoning involved forming traditional approaches such as rule-based heuristics in the form of symbolic representations (Carpenter, Just, and Shell 1990; Lovett and Forbus 2017; Lovett, Forbus, and Usher 2010; Lovett et al. 2009) or relational structures in the images (Little, Lewandowsky, and Griffiths 2012; McGregor and Goel 2014; Mekik, Sun, and Dai 2018). These methods were limited in their capability of ever completely understanding the full reasoning tasks due to the following underlying assumption made by them. The first limitation in the experiments was assuming the machines of having access to the symbolic representation from images, and inferring rules based on them. Next, the need for a domain expertise that understands the operations and the comparisons required in design principles in these reasoning tasks. The possibility of ever fully understanding and solving these task was made possible when (Wang and Su 2015) proposed their systematic way of automatically generating RPM using first-order logic. Recently, there has been a growing interest in using deep neural networks to solve abstract reasoning because of their ability to learn powerful representations directly from the images. Since then, there has been significant progress in solving reasoning tasks using neural networks. Hoshen and Werman (Hoshen and Werman 2017) employed a CNN to find the matching choice for the 3×3 context images, while (Barrett et al. 2018) proposed a Wild Relational Network (WReN) to study the nature of relationships between context and choice images.

Disentanglement. Over these recent years research in learning disentangled representation is gaining momentum (Bengio, Courville, and Vincent 2013; Higgins et al. 2016; Kim and Mnih 2018; Kim et al. 2019a,b; Locatello et al. 2019a; Ridgeway 2016; Tschannen, Bachem, and Lucic 2018). However, with all the proposed works this research area has not reached a major consensus on two major notions: i) there is no widely accepted formalized definition (Bengio, Courville, and Vincent 2013; Ridgeway 2016; Locatello et al. 2019a; Tschannen, Bachem, and Lucic 2018), ii) no single robust evaluations metrics to compare the models (Burgess et al. 2018; Kim and Mnih 2018; Chen et al. 2018; Eastwood and Williams 2018; Kumar, Sattigeri, and Balakrishnan 2018). However, the key fact common to all the models claim to learn disentangled representation is the extraction of statistically independent (Ridgeway 2016) learned factors. A majority of the research in this area is based on the definition presented by (Bengio, Courville, and Vincent 2013), which states that the underlying generative factors correspond to independent latent dimensions, such that changing a single factor of variation

should change only a single latent dimension while remaining invariant to others. In a recent work, (Locatello et al. 2019a) proposed the theoretical impossibility result which states it is impossible to learn disentangled representation without the presence of inductive bias. There is a shift towards semi-supervised (Locatello et al. 2019b; Sorrenson, Rother, and Köthe 2020; Khemakhem et al. 2020) and weak-supervised (Locatello et al. 2020; Bouchacourt, Tomioka, and Nowozin 2018; Hosoya 2018; Shu et al. 2019) based disentangling models.

In this work, we focus on both learning disentangled representation as well solving abstract visual reasoning. A large scale study by (van Steenkiste et al. 2019) showed using previous state-of-the-art (SOTA) disentangled models that disentangled representation are helpful in solving reasoning tasks. We focus on using the inductive bias present in the reasoning questions to jointly optimize both the tasks. Following section In the section below, we start by propping a general framework to solve abstract reasoning and a novel model design (DAReN), followed by empirical results comparing DAReN with previous SOTA methods.

3 Problem Formulation and Approach

We first describe the Raven’s Progressive Matrices that forms our visual reasoning task in Section 3.1. We then propose our general generative graphical model for RPM, *GM-RPM*, which will form the essential basis for inductive bias in joint learning for representation and reasoning in Section 3.2. Finally, in Section 3.3, we describe our novel learning framework based on a variational autoencoder (VAE) and a reasoning network for jointly representation-reasoning learning.

3.1 Visual Reasoning Task

The Raven’s matrix denoted as \mathcal{M} , of size $M \times M$ contains images at all m, j location except at \mathcal{M}_{MM} . The aim is to find the best fit image at \mathcal{M}_{MM} from a list of choices denoted as A . For our current work, we have fixed $M = 3$, where $\mathcal{M} = \{x_{11}, \dots, x_{32}\}$ in row-major order and \mathcal{M}_{33} is empty that needs to be placed with the correct image from the choices. We also set the number of choices $|A| = 6$, where $A = \{a_1, \dots, a_6\}$.

We formulate an abstract representation for all patterns possible in \mathcal{M} by defining a structure S on the image attributes (o) and on relation types (r) applied to the image attributes

$$S = \{(r, o) : r \in R \text{ and } o \in O\}.$$

The set R consists of relations proposed by (Carpenter, Just, and Shell 1990) that are constant in a row, quantitative pairwise progression, figure addition or subtraction, distribution of three values, and distribution of two values. We describe our approach below by assuming these relationships on the rows of RPM. The procedure remains the same for modeling relationships on the columns of RPM. Similarly, the image attributes (O) set consists of object type, size, position, and color. These image attributes are usually the K underlying generative factors in the images. The structure S is a set of

tuples, where each tuple is formed by randomly sampling a relation from R and image attribute from O . The set of S can contain a max of $|R| * |O|$ tuple, where the difficulty rises with the increase in the size of R , O or $|S|$ or any combination of them. Finally, the matrix \mathcal{M} is created using the tuples in S . For the matrix \mathcal{M} to be a valid RPM an additional required consistency constraint is described below.

RPM Constraint. Using S , multiple realizations of the matrix \mathcal{M} are possible depending on the randomly sampled values of (r, o) . For example, if $S = \{(\text{constant in a row, object type}), (\text{constant in a row, object size})\}$, every image in each row or column of \mathcal{M} will have the same (constant) value for $o = \{\text{object type, object size}\}$ ¹. The values for image attributes in $\bar{o} = O \setminus o$, that are not part of S , are sampled randomly for every image. These sampled values must not comply with the relation set $r \in S$ across all rows or columns in \mathcal{M} . In the example above where $\bar{o} = \{\text{position, color}\}$, a valid \mathcal{M} can also have same values for position or color (or both) in the first row while the values in the other two rows have to be different (not to contradict S). The above is an example of a distractor, where the attributes in \bar{o} during the sampling process might satisfy some $(r, o) \in S$ for any one row in \mathcal{M} but not for all M rows. These randomly varying values in \bar{o} add a layer of difficulty towards solving RPM.

The task of any model trained to solve \mathcal{M} has to find r that is consistent across all rows or columns in \mathcal{M} and discard the distracting features \bar{o} . In the rest of the paper, for simplicity we work on row based relationship on RPM. Our solution could easily be extended to address columns or both rows and columns.

3.2 Inductive Prior for RPM (GM-RPM)

While previous works have made strides in solving RPMs (Little, Lewandowsky, and Griffiths 2012; Lovett and Forbus 2017; van Steenkiste et al. 2019), the gap in reasoning and representation learning between those approaches and the human performance remains. To narrow this gap we propose a minimal inductive bias in the form of a probabilistic graphical model described here that can be used to guide the joint representation-reasoning learning. Figure 2 defines the structure of the general generative graphical model for RPM. This model describes an RPM $\mathcal{M} = \{x_{11}, \dots, x_{M,M}\}$, where $x_{mj}, m = 1, \dots, M, j = 1, \dots, M$, denote the images in the puzzle, with the correct answer at $x_{M,M}$, defined by rule r on the subset of K possible attributes indexed by the multi-hot attribute selection vector $o \in \{0, 1\}^K$.

Latent vectors $z_{mj} \in \mathbb{R}^{K+N}$ are the representations of the K attributes, to be learned by our approach, and some inherent noise process encompassed in the remaining N dimensions of $z_{mj}, z_{mj,n} \in \mathbb{R}^N$, which we refer to as nuisances. Ideally, some K factors in z_{mj} should be isomorphic to the attributes themselves in this simple RPM setting, after an optimal model is learned. This latent vector of gives rise to ambient images through some stochastic nonlinear map-

¹We interchangeably use o to denote the subset of image attributes that adhere to rules of RPM as well as the multi-hot vector $o \in \{0, 1\}^K$ whose non-zero values index those attributes.

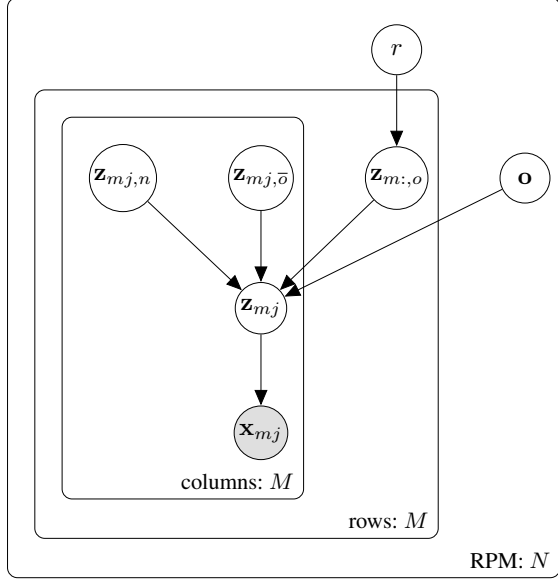


Figure 2: Generative models for RPM (GM-RPM). See Sec. 3.2 for details.

ping $x \sim p(x|f(z|\Theta))^2$, parameterized by Θ which is to be learned,

$$p(\mathcal{M}|\mathbf{Z}, \Theta) = \prod_m \prod_j p(\mathbf{x}_{mj}|f(\mathbf{z}_{mj}|\Theta)), \quad (1)$$

where $\mathbf{Z} = [\mathbf{z}_{mj}]_{M \times M} \in \mathbb{R}^{M \times M \times (K+N)}$ is the latent tensor for the RPM.

The RPM inductive bias comes from the way (prior) \mathbf{z}_{mj} are formed, given the unknown rule r . Specifically,

$$\mathbf{z}_{mj} = \begin{bmatrix} \mathbf{o} \odot \mathbf{z}_{mj,o} + \bar{\mathbf{o}} \odot \mathbf{z}_{mj,\bar{o}} \\ \mathbf{z}_{mj,n} \end{bmatrix} \quad (2)$$

where $\bar{\mathbf{o}} = \mathbf{1} - \mathbf{o}$, $\mathbf{z}_{mj,o} \in \mathbb{R}^K$ is the latent representation of the factors that are used in rule r and $\mathbf{z}_{mj,\bar{o}} \in \mathbb{R}^K$ is the latent representation of the complementary, unused factors. The key in RPM is how the priors on those factors are defined. The factors used in the rule, grouped as the tensor $\mathbf{Z}_o = [\mathbf{z}_{mj,o}]_{M \times M}$, follow some joint density over elements $j = 1, \dots, M$ of the same row m

$$p(\mathbf{Z}_o|r) = \prod_m p(\mathbf{z}_{m:,o}|r) = \prod_m p(\mathbf{z}_{m1,o}, \dots, \mathbf{z}_{mM,o}|r), \quad (3)$$

where $\mathbf{z}_{m:,o}$ is the matrix of size $K \times M$ or all latent representations in row m of RPM. The factors *not* used in the rule, $\bar{\mathbf{o}}$, have a different, iid prior

$$p(\mathbf{Z}_{\bar{o}}|r) = \prod_m \prod_j p(\mathbf{z}_{mj,\bar{o}}). \quad (4)$$

This is depicted by the inner-most plate, “columns: M”, in Figure 2. Finally, the factors representing the noise informa-

²We drop RPM indices, where obvious.

tion have iid prior

$$p(\mathbf{Z}_n) = \prod_m \prod_j \mathcal{N}(\mathbf{z}_{mj,n}; 0, I). \quad (5)$$

Additionally, we assume that all $K + N$ factors are independent in those used for the puzzle, those not used, and the nuisances,

$$p(\mathbf{z}_{m:,o}|r) = \prod_k p(\mathbf{z}_{m:,o}^k|r)$$

$$p(\mathbf{z}_{mj,\bar{o}}) = \prod_k p(\mathbf{z}_{mj,\bar{o}}^k)$$

$$p(\mathbf{z}_{mj,n}) = \prod_k p(\mathbf{z}_{mj,n}^k)$$

This finally gives rise to the full Generative models for RPM (GM-RPM),

$$P(\mathcal{M}; \mathbf{Z}, \mathbf{Z}_o, \mathbf{Z}_{\bar{o}}, \mathbf{Z}_n, r, \mathbf{o}) = p(\mathcal{M}|\mathbf{Z})p(\mathbf{Z}|\mathbf{Z}_o, \mathbf{Z}_{\bar{o}}, \mathbf{Z}_n, \mathbf{o})p(\mathbf{Z}_o|r)p(\mathbf{Z}_{\bar{o}})p(\mathbf{Z}_n). \quad (6)$$

3.3 Representation and Reasoning: DAREn

Inspired by our *GM-RPM*, we propose a novel framework for learning representation and reasoning named **Disentangling based Abstract Reasoning Network (DAREn)**. Please refer to Figure 3 for an overview of DAREn.

DAREn is composed of two primary components, a variational auto encoder (VAE) module and a reasoning module. The encoder model encodes the matrix \mathcal{M} (without the last element) into latent representation $\mathbf{Z} \in \mathbb{R}^{(M^2-1) \times (K+N)}$, whose structure assumes that in (2), and the choice list A as $\mathbf{Z}_A = \{Z_{a_i}\}, i \in \{1, 6\}$, respectively. The latent variables \mathbf{Z} and \mathbf{Z}_A are used as input to both disentangling and reasoning module. In the case of disentangling module, we use an averaging strategy on the subset of K underlying factors with $\mathbf{o} = 1$. The updated latent variable is given to the decoder model to reconstruct the original images. The input to the reasoning module is prepared by changing the tensor dimension of \mathbf{Z} to $\mathbb{R}^{M \times M \times (K+N)}$, where a choice Z_{a_i} is placed at (M, M) location in \mathbf{Z} . The reasoning network outputs a choice probability score for each choice a_i , where i with the highest value is predicted as the best fit image by the reasoning network. In the following section, we describe the disentanglement learning using VAE followed by the reasoning module.

Inference. Our proposed generative model uses a VAE (Kingma and Welling 2013) to learn the disentangled representations. As described in Section 3.2, the goal is to infer the value of the latent variables that generated the observations, i.e., to calculate the posterior distribution over $p(\mathbf{Z}, \mathbf{o}, r|\mathcal{M})$, which is intractable. Instead, an approximate solution for the intractable posterior was proposed by (Kingma and Welling 2013) that uses a variational approximation $q(\mathbf{Z}, \mathbf{o}, r|\mathcal{M}; \phi)$, where ϕ are the variational parameters. In this work, we further define this variational posterior

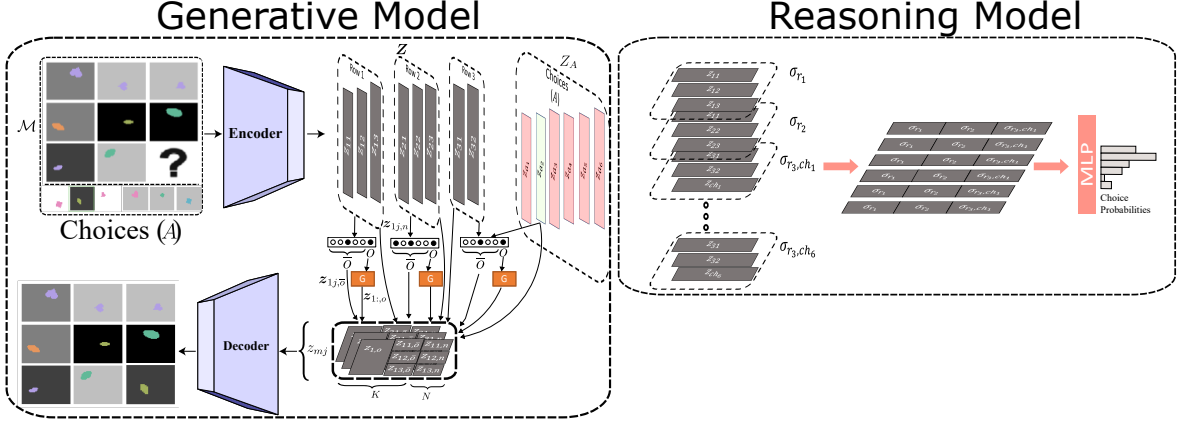


Figure 3: Illustration of **DAREn**. Our novel learning framework consists of a VAE-based generative model (left) and a reasoning network (right). **Generative Model**. The encoder encodes \mathcal{M} and A to \mathbf{Z} and \mathbf{Z}_A . The K possible attributes are learnt from \mathcal{M} by picking the factor indices with high variance and the rest are kept as nuisances (N). The set bits for \mathbf{o} (shown as a multi hot vector) for row m is obtained from fixed factor constraint. No operation is performed on the factor indices at the set bit of \bar{o} and the nuisance factors. The factor indices in the set bit of \mathbf{o} are enforced by rule constraint to take the same value via an averaging strategy (G). The updated latent representation is given to the decoder to reconstruct the image back. **Reasoning Model**. We consider the latent representation \mathbf{Z} and \mathbf{Z}_A to extract the standard deviation across factor index for the top two rows and all possible 6 rows. An MLP is trained on the concatenated standard deviation of the top two rows with choice a_i to predict the best fit choice image.

as

$$q(\mathbf{Z}, \mathbf{o}, r | \mathcal{M}; \phi) \propto q_r(r | \mathbf{Z}) \rho(\mathbf{Z}, \mathbf{Z}') q_o(\mathbf{o} | \mathbf{Z}') \prod_{m,j} q_\phi(\mathbf{z}'_{mj} | \mathbf{x}_{mj}). \quad (7)$$

Currently, DAREn is designed to solve for $r = \text{constant}$ in a row, thus $q_r(r | \mathbf{Z}) = \delta(r - r_{\text{const}})$. \mathbf{Z}' is an intermediate variable, which is used to arrive at the final estimate of \mathbf{Z} , using the Rule Enforcing Constraint function $\rho(\cdot, \cdot)$, as described further in this section. We use the inductive bias in Sec. 3.2 to define $q_o(\mathbf{o} | \mathbf{Z}') = \delta(\mathbf{o} - \hat{\mathbf{o}}(\mathbf{Z}'))$ as described below.

Disentangling Module. Initial inference of latent factors, \mathbf{Z} , is accomplished using the disentangling VAE encoder from (Tschannen, Bachem, and Lucic 2018), which uses the following general ELBO optimization

$$\mathcal{L}_{DVAE} = \max_{\theta, \phi} E_{p(x)} \left[E_{q_\phi(z|x)} [\log p_\theta(x|z)] - \lambda_1 R_1(q_\phi(z|x)) - \lambda_2 R_2(q_\phi(z)) \right] \quad (8)$$

Here, regularizer R_1 controls the information flow in $q(z|x)$, regularizer R_2 induces the disentanglement on the latent representation and the hyperparameter λ_1, λ_2 controls the weight on each of the regularizers. Most of the regularization based disentangling work can be subsumed into the above objective form.

Weak Supervision via RPM Structure. We use the inductive bias present in \mathcal{M} via S to guide our disentangling module. We describe the approach to infer K possible attributes

from $\mathbf{z} \in \mathbb{R}^{K+N}$. We initialize the variational parameters ϕ using a partial pre trained network and then use \mathbf{Z} to compute the variance across each factor index. The values for the variance above a certain threshold ($\epsilon = 0.05$) are considered K factors and the rest the N nuisances.

Enforcing Fixed Factor Constraint We infer the set bits of \mathbf{o} for a given \mathcal{M} from prior in (3), where the image attributes share the same value for the set bits of \mathbf{o} for row m . We compute the KL divergence over the latent vectors in \mathcal{M} and extract the indices of l -lowest divergence values as our \mathbf{o} .

$$\begin{aligned} \overline{KL}_m &= \frac{1}{M^2} \sum_{1 \leq i,j \leq M} KL(q_\phi(\mathbf{z}_{mi} | \mathbf{x}_{mi}) || q_\phi(\mathbf{z}_{mj} | \mathbf{x}_{mj})) \\ \overline{KL}_{\mathcal{M}} &= \frac{1}{M} \sum_{m=1}^M \overline{KL}_{\text{row}_m} \end{aligned} \quad (9)$$

where i, j represents the indices in row m . The KL divergence over \mathcal{M} denoted as $\overline{KL}_{\mathcal{M}} \in \mathbb{R}^K$ is used to determine whether the factor at k^{th} index is consistent in \mathcal{M} . The set \mathbf{o} consists of indices with values lower than $\frac{1}{K} \sum \overline{KL}_{\mathcal{M}}$. In the empirical study, we fix $|\mathbf{o}| = 1$, so $\hat{o}_k = \min_k \overline{KL}_{\mathcal{M}}$.

Enforcing Rule Constraint. We describe the process of preparing the estimated latent variable \mathbf{z}'_{mj} . The averaging strategy is applied to latent vector \mathbf{Z}_o . We use the set values of \mathbf{o}_k extracted from above to enforce the relation r on the images in row m , where as for $\bar{o} = 1$ and noise indices N

the values remains unchanged in Z .

$$z'_{mj} = \begin{cases} f_{avg}(\{z_{m1,o} \dots z_{mM,o}\}), & \text{where } o = 1 \\ z_{mj}, & \text{otherwise} \end{cases}$$

For $r = \text{constant}$ in a row, the averaging strategy is variant of the method in Multi Level VAE (Bouchacourt, Tomioka, and Nowozin 2018) to obtain \hat{z}_{mj}

$$f_{avg}(z'_{mj,o}) = \frac{1}{M} \sum_{j=1}^M z_{mj,o} \quad (10)$$

The final latent vector is prepared as per (2).

From above constraints, we obtain new representations for each in \mathcal{M} denoted as z'_{mj} where the attributes o from S are constrained by r . The decoder network maps z'_{mj} to original image. Since the attributes o vary across \mathcal{M} , the above constraints forces the model to keep the factors separate which improves disentangling.

3.4 Reasoning Module

The reasoning component of DAREN incorporates a relational structure to infer the abstract relationship on the attribute o for images in \mathcal{M} . The input to our reasoning module is the disentangled latent variables of \mathcal{M} and A . We prepare $|A|$ possible last rows by placing each choice image in A at the missing location $\mathcal{M}_{3,3}$. Given \mathcal{M} , it is known that the correct image will satisfy r in the last row, where r is already true for the top $M - 1$ rows. To determine the correct choice, we contrast the values at k^{th} index in z_m by computing the variance over all images at row m . Using the above step, we compute the variance for all $M + A - 1$ rows that includes all $|A|$ probable last rows. Additionally, we append a positional encoding at the end of each row wise variance computed above. In the next step, we concatenate the variance in latent variables for the top $M - 1$ rows along with each possible last row to prepare $|A|$ choice vectors ($\mathbb{R}^{|A| \times M \times D}$). Finally, we train a basic three-layered MLP to process each choice vectors from above to produce a logit vector of size $|A|$. The choice with the highest score is selected as the correct answer. We train the reasoning model using CrossEntropy loss.

4 Experiments

4.1 Datasets

We study the performance of DAREN on six datasets - (i) *dsprites* (Matthey et al. 2017), (ii) modified *dSprites* (van Steenkiste et al. 2019), (iii) *shapes3d* (Kim and Mnih 2018), (iv-vi) MPI3D - (Real, Realistic, Toy) (Gondal et al. 2019). We use similar experimental settings as proposed in (van Steenkiste et al. 2019) to create RPM for the above datasets. Please see Appendix for the description of the datasets and the details on the preparation of the RPMs. We compare our results in both the reasoning accuracy and the disentanglement scores against the SOTA methods. For both categories, we show that our model outperforms SOTA approaches.

4.2 Experimental Setup, Baselines and Evaluation Metric

For our experiments, we used the objectives proposed in Factor-VAE (Kim and Mnih 2018) as replacement of the regularizers in (8) for the disentangled module. In case of Factor-VAE, the information flow regularizer is $KL(q_\phi(z|x)||p(z))$ and the disentanglement regularizer is $KL(q(z)||\prod_{k=1}^d q(z_k))$. All our models are implemented in PyTorch (Paszke et al. 2019) and optimized using ADAM optimizer (Kingma and Ba 2014), with the following parameters: learning rate of $1e-4$ for the reasoning + representation network excluding the Discriminator of Factor-VAE which is set to $1e-5$. To demonstrate that our approach is less sensitive to the choice of the hyper-parameters (γ), and network initialization, we sweep over 35 different hyper parameter settings of $\gamma \in \{1.0, 10.0, 20.0, 30.0, 40.0, 50.0, 100.0\}$ and initialization seeds $\{1, 2, 3, 4, 5\}$. We kept the architecture and other hyperparameters similar to the experiments in (van Steenkiste et al. 2019). The image size used in all six datasets is $64 \times 64 \times 3$ pixels. The pixel intensity was scaled to $[0,1]$. We use a batch size of 64 during the training process.

Baselines. We refer to the training process in (van Steenkiste et al. 2019) as *Staged-WReN* for convenience. With the above settings, we evaluate DAREN against *Staged-WReN* for abstract reasoning task and against Factor-VAE for disentangled representation learning. The *Staged-WReN* method was a two stage training process, where a disentangling network was trained first ($\sim 300K$ iterations), followed by training a Wild Relational Network (WReN) proposed by (Barrett et al. 2018) on RPM using the fixed disentangled representation from the encoder trained for $300K$. Similar, we use the weights of a partially pre-trained model to initialize our VAE model. However, we start at a lower starting point ($\sim 200K$) compared to *Staged-WReN* and train DAREN for 100K iterations.

We propose an adapted baseline referred to as *E2E-WReN* over *Staged-WReN*, where we train both the disentangling and the reasoning network jointly end-to-end. We adopt the similar notation used in (van Steenkiste et al. 2019) where the context panels $C = \{x_1, \dots, x_8\}$ and answer panels $A = \{a_1, \dots, a_6\}$. WReN is evaluated for each answer panel $a \in A$ in relation to the context panels. The following presents the learning objective of *E2E-WReN*

$$\arg \max_k f_\phi \left(\sum_{i,j \leq M \times M} g_\theta(Z_k(i), Z_k(j)) \right), \\ Z_k = [z(x_1), z(x_2), \dots, z(x_8), z(a)], a \in A. \quad (11)$$

which is similar to *Staged-WReN*. However, *E2E-WReN* trains the the VAE module as well. Please refer appendix for a detailed description on *E2E-WReN*.

4.3 Analyzing Abstract Visual Reasoning Results

We report the performance as mean \pm variance of reasoning accuracy (refer Table 1) over 6 benchmark datasets. We start by comparing *Staged-WReN* against the adapted baseline (*E2E-WReN*). We observe an increase of $\sim 2 - 17\%$

Table 1: Performance (mean \pm variance) of reasoning accuracy on the 6 benchmark dataset. Note that the higher the better. The best score for each dataset among the competing models are shown in bold red and second-best in blue. (Note: * values are taken from (van Steenkiste et al. 2019).)

Model/Dataset	DSprites	Modified DSprites	Shapes3D	MPI3D-Real	MPI3D-Realistic	MPI3D-Toy
<i>Staged-WReN</i> (van Steenkiste et al. 2019)	97.4 \pm 4.2	80.0*	90.0*	61.6 \pm 9.4	55.5 \pm 8.1	64.2 \pm 13.3
E2E-WReN	99.6 \pm 0.5	85.7 \pm 11.4	98.3 \pm 2.0	72.2 \pm 8.8	72.7 \pm 7.5	80.8 \pm 3.5
DAReN	99.3 \pm 0.5	86.5 \pm 10.4	99.2 \pm 0.8	74.3 \pm 9.9	73.5 \pm 6.5	81.5 \pm 6.8

in performance from *Staged-WReN* to *E2E-WReN* which supports our hypothesis that better representation results in improved reasoning performance. The WReN learns a relational structure by aggregating all pair-wise relations formed within the context panels and between context and choice panels in the latent space to find the best-fit choice image for the context. Since the working procedure over *Staged-WReN* and *E2E-WReN* remain similar, the difference in reasoning performance is credited to the presence of stronger signals in the latent representation for *E2E-WReN* that back-propagate from the reasoning module. Despite this, WReN performance is sub-optimal in learning the underlying reasoning patterns. One reason is that the pairwise relations formed between the context panels do not contribute towards predicting any choice because the values in these pairwise relations remain the same across all choice panels. Consequently, a trained WReN learns to ignore within-context pairwise comparisons. Only the pairwise score between context panels and each choice panel is used for inferring the relationship. We have empirically verified this on both trained networks (*Staged-WReN* and *E2E-WReN*) over all the datasets, where the scores of non-interfering comparisons across all choices do not impact the final prediction by the model. A detailed analysis of the empirical results is provided in the appendix. This blind formulation of pairwise relation presents a major downside to the quality of learning in WReN. We can observe from *GM-RPM*, that relation r bounds the image attributes o in a row-wise manner, hence any pairwise comparison between a choice panel (including correct image) and context panel in the top $M - 1$ rows does not help in learning r or o . This can be seen with an example, where $r = \text{constant}$ in a row, the pairwise comparison performed between context panel in the top $M - 1$ rows with a choice panel (including correct answer) can never have the same values for o . Due to the above reason forming every possible pairwise relation hinders model learning. In our DAReN, we avoid forming general pairwise combinations instead use our *GM-RPM* to model (r, o) . The results of DAReN outperform *E2E-WReN* for all datasets. Our results on these datasets provide evidence of stronger affinity between reasoning and disentanglement, which DAReN is able to exploit.

4.4 Analyzing Disentangling Results

As illustrated above, while learning the relations DAReN also separates the underlying latent factors. In Table 2, we report the disentanglement scores of trained models on five widely used evaluation metrics namely, β -VAE met-

ric (Higgins et al. 2016), Factor-VAE metric (Kim and Mnih 2018), DCI disentanglement (Eastwood and Williams 2018), MIG (Chen et al. 2018), and SAP-Score (Kumar, Sattigeri, and Balakrishnan 2018). We compare the latent representation learnt for all three models at 300K iteration. As described in Section 4.3, a joint learning framework not only improves reasoning performance but also strongly disentangles the latent vector in contrast to Factor-VAE, an unsupervised (reasoning-free) approach. *E2E-WReN* improves upon it but is still suboptimal in disentangling the latent factors, as observed in Table 2. One major reason for large improvements by DAReN compared to Factor-VAE and even *E2E-WReN* is due the extraction of K underlying generative factors and the averaging strategy over the least varying index in K . Generally during the unsupervised training process, indices of nuisance factor might receive weak signals from the true generative factors. However, DAReN removes this infusion of true signals with the nuisance factors by separating o and n .

Table 2: Disentanglement Metrics on the 6 benchmark datasets. Performance (mean \pm variance) of disentanglement score widely used metric.

	Model	β -VAE	F-VAE	DCI	MIG	SAP
DSprites	F-VAE	85.9 \pm 6.2	74.4 \pm 7.3	52.9 \pm 10.5	28.7 \pm 11.5	4.0 \pm 1.4
	E2E-WReN	86.9 \pm 2.8	77.6 \pm 5.0	58.1 \pm 8.0	38.2 \pm 7.7	6.0 \pm 2.2
	DAReN	87.8 \pm 2.1	79.2 \pm 6.2	59.0 \pm 6.4	39.0 \pm 0.0	6.0 \pm 2.0
Mod DSprites	F-VAE	51.4 \pm 13.8	44.0 \pm 10.6	31.2 \pm 7.6	13.8 \pm 7.1	6.4 \pm 2.6
	E2E-WReN	75.2 \pm 10.0	65.1 \pm 10.6	43.0 \pm 6.9	26.1 \pm 9.1	8.3 \pm 3.3
	DAReN	87.6 \pm 11.6	77.0 \pm 13.2	50.1 \pm 11.3	34.9 \pm 12.4	12.6 \pm 4.8
Shapes3D	F-VAE	91.9 \pm 5.9	84.5 \pm 8.7	73.9 \pm 9.0	44.6 \pm 18.8	6.3 \pm 2.9
	E2E-WReN	94.2 \pm 4.7	91.3 \pm 6.5	79.1 \pm 7.7	54.9 \pm 15.7	8.4 \pm 3.8
	DAReN	99.9 \pm 0.3	98.4 \pm 3.2	91.6 \pm 4.7	68.8 \pm 17.5	17.2 \pm 4.8
Realistic	F-VAE	61.7 \pm 6.9	45.0 \pm 5.5	37.4 \pm 4.6	22.7 \pm 7.7	9.8 \pm 2.6
	E2E-WReN	70.7 \pm 5.8	55.3 \pm 6.1	42.5 \pm 6.4	29.7 \pm 8.1	12.8 \pm 2.9
	DAReN	87.8 \pm 7.9	75.8 \pm 8.6	50.6 \pm 5.9	36.1 \pm 8.2	19.3 \pm 5.2
Real	F-VAE	71.6 \pm 8.7	57.8 \pm 7.5	46.1 \pm 2.5	31.2 \pm 6.1	14.4 \pm 4.0
	E2E-WReN	78.4 \pm 7.6	65.0 \pm 7.3	48.0 \pm 3.5	34.3 \pm 7.0	18.2 \pm 4.4
	DAReN	90.0 \pm 10.0	75.8 \pm 9.7	51.8 \pm 4.9	37.0 \pm 8.1	20.8 \pm 5.3
Toy	F-VAE	67.4 \pm 5.0	49.2 \pm 4.1	43.0 \pm 2.5	29.7 \pm 7.0	10.6 \pm 2.4
	E2E-WReN	75.3 \pm 4.3	58.6 \pm 4.2	48.0 \pm 2.9	37.8 \pm 7.9	13.7 \pm 2.9
	DAReN	87.6 \pm 14.2	75.3 \pm 15.4	52.8 \pm 6.8	35.1 \pm 9.6	18.7 \pm 5.5

5 Conclusion

In this paper, we introduce an end-to-end learning framework to jointly learn the representation and reasoning using inductive bias as a weak form of supervision in Raven’s Progressive Matrices. To this end, we propose a general gener-

ative graphical model for RPM (*GR-RPM*) as a prior for the reasoning task. We realize a new joint learning framework DAREn based on the principles defined in *GR-RPM*. Our DAREn is composed of two components – a disentangling network and a reasoning network. Our disentangling network allows easy integration of different representation learning frameworks. We fix the relation r and evaluate our model DAREn on six benchmark datasets to measure the performance of reasoning and disentangling. Abstract visual reasoning task is hard problem in the presence of latent generative factors K , relation r , and image attributes o . We show evidence of strong correlation between the two learning disentangled representation and solving the reasoning tasks. The general nature of *GR-RPM* and DAREn opens further possibilities for research in joint learning of representation and reasoning, including generalization to arbitrary relationship.

References

- Barrett, D.; Hill, F.; Santoro, A.; Morcos, A.; and Lillicrap, T. 2018. Measuring abstract reasoning in neural networks. In *International Conference on Machine Learning*, 511–520.
- Bengio, Y.; Courville, A.; and Vincent, P. 2013. Representation learning: A review and new perspectives. *IEEE transactions on pattern analysis and machine intelligence*, 35(8): 1798–1828.
- Bouchacourt, D.; Tomioka, R.; and Nowozin, S. 2018. Multi-level variational autoencoder: Learning disentangled representations from grouped observations. In *Thirty-Second AAAI Conference on Artificial Intelligence*.
- Bringsjord, S.; and Schimanski, B. 2003. What is artificial intelligence? Psychometric AI as an answer. In *IJCAI*, 887–893. Citeseer.
- Burgess, C. P.; Higgins, I.; Pal, A.; Matthey, L.; Watters, N.; Desjardins, G.; and Lerchner, A. 2018. Understanding disentangling in β -VAE. *arXiv preprint arXiv:1804.03599*.
- Carpenter, P. A.; Just, M. A.; and Shell, P. 1990. What one intelligence test measures: a theoretical account of the processing in the Raven Progressive Matrices Test. *Psychological review*, 97(3): 404.
- Chen, R. T. Q.; Li, X.; Grosse, R.; and Duvenaud, D. 2018. Isolating Sources of Disentanglement in Variational Autoencoders. In *Advances in Neural Information Processing Systems*.
- Eastwood, C.; and Williams, C. K. 2018. A framework for the quantitative evaluation of disentangled representations. In *International Conference on Learning Representations*.
- Gondal, M. W.; Wuthrich, M.; Miladinovic, D.; Locatello, F.; Breidt, M.; Volchkov, V.; Akpo, J.; Bachem, O.; Schölkopf, B.; and Bauer, S. 2019. On the Transfer of Inductive Bias from Simulation to the Real World: a New Disentanglement Dataset. *Advances in Neural Information Processing Systems*, 32: 15740–15751.
- Higgins, I.; Matthey, L.; Pal, A.; Burgess, C.; Glorot, X.; Botvinick, M.; Mohamed, S.; and Lerchner, A. 2016. beta-vae: Learning basic visual concepts with a constrained variational framework.
- Hoshen, D.; and Werman, M. 2017. Iq of neural networks. *arXiv preprint arXiv:1710.01692*.
- Hosoya, H. 2018. Group-based learning of disentangled representations with generalizability for novel contents. *arXiv preprint arXiv:1809.02383*.
- Khemakhem, I.; Kingma, D.; Monti, R.; and Hyvarinen, A. 2020. Variational autoencoders and nonlinear ica: A unifying framework. In *International Conference on Artificial Intelligence and Statistics*, 2207–2217. PMLR.
- Kim, H.; and Mnih, A. 2018. Disentangling by Factorising. In *International Conference on Machine Learning*, 2649–2658.
- Kim, M.; Wang, Y.; Sahu, P.; and Pavlovic, V. 2019a. Bayes-factor-vae: Hierarchical bayesian deep auto-encoder models for factor disentanglement. In *Proceedings of the IEEE/CVF International Conference on Computer Vision*, 2979–2987.
- Kim, M.; Wang, Y.; Sahu, P.; and Pavlovic, V. 2019b. Relevance factor VAE: Learning and identifying disentangled factors. *arXiv preprint arXiv:1902.01568*.
- Kingma, D. P.; and Ba, J. 2014. Adam: A method for stochastic optimization. *arXiv preprint arXiv:1412.6980*.
- Kingma, D. P.; Mohamed, S.; Rezende, D. J.; and Welling, M. 2014. Semi-supervised learning with deep generative models. In *Advances in neural information processing systems*, 3581–3589.
- Kingma, D. P.; and Welling, M. 2013. Auto-encoding variational bayes. *arXiv preprint arXiv:1312.6114*.
- Klein, B.; Raven, J.; and Fodor, S. 2018. Scrambled Adaptive Matrices (SAM)—A new test of eductive ability. *Psychological Test and Assessment Modeling*, 60(4): 451.
- Kumar, A.; Sattigeri, P.; and Balakrishnan, A. 2018. Variational Inference of Disentangled Latent Concepts from Unlabeled Observations. In *International Conference on Learning Representations*.
- Little, D. R.; Lewandowsky, S.; and Griffiths, T. L. 2012. A Bayesian model of rule induction in Raven’s Progressive Matrices. In *Proceedings of the Annual Meeting of the Cognitive Science Society*, volume 34.
- Locatello, F.; Bauer, S.; Lucic, M.; Raetsch, G.; Gelly, S.; Schölkopf, B.; and Bachem, O. 2019a. Challenging common assumptions in the unsupervised learning of disentangled representations. In *international conference on machine learning*, 4114–4124. PMLR.
- Locatello, F.; Poole, B.; Rätsch, G.; Schölkopf, B.; Bachem, O.; and Tschannen, M. 2020. Weakly-supervised disentanglement without compromises. In *International Conference on Machine Learning*, 6348–6359. PMLR.
- Locatello, F.; Tschannen, M.; Bauer, S.; Rätsch, G.; Schölkopf, B.; and Bachem, O. 2019b. Disentangling Factors of Variations Using Few Labels. In *International Conference on Learning Representations*.
- Lovett, A.; and Forbus, K. 2017. Modeling visual problem solving as analogical reasoning. *Psychological review*, 124(1): 60.

- Lovett, A.; Forbus, K.; and Usher, J. 2007. Analogy with qualitative spatial representations can simulate solving Raven’s Progressive Matrices. In *Proceedings of the Annual Meeting of the Cognitive Science Society*, volume 29.
- Lovett, A.; Forbus, K.; and Usher, J. 2010. A structure-mapping model of Raven’s Progressive Matrices. In *Proceedings of the Annual Meeting of the Cognitive Science Society*, volume 32.
- Lovett, A.; Tomai, E.; Forbus, K.; and Usher, J. 2009. Solving geometric analogy problems through two-stage analogical mapping. *Cognitive science*, 33(7): 1192–1231.
- Matthey, L.; Higgins, I.; Hassabis, D.; and Lerchner, A. 2017. dsprites: Disentanglement testing sprites dataset. URL <https://github.com/deepmind/dsprites-dataset/>. [Accessed on: 2018-05-08].
- McGreggor, K.; and Goel, A. 2014. Confident reasoning on Raven’s progressive matrices tests. In *Twenty-Eighth AAAI Conference on Artificial Intelligence*.
- Mekik, C. S.; Sun, R.; and Dai, D. Y. 2018. Similarity-Based Reasoning, Raven’s Matrices, and General Intelligence. In *IJCAI*, 1576–1582.
- Paszke, A.; Gross, S.; Massa, F.; Lerer, A.; Bradbury, J.; Chanan, G.; Killeen, T.; Lin, Z.; Gimelshein, N.; Antiga, L.; Desmaison, A.; Kopf, A.; Yang, E.; DeVito, Z.; Raison, M.; Tejani, A.; Chilamkurthy, S.; Steiner, B.; Fang, L.; Bai, J.; and Chintala, S. 2019. PyTorch: An Imperative Style, High-Performance Deep Learning Library. In Wallach, H.; Larochelle, H.; Beygelzimer, A.; d’Alché-Buc, F.; Fox, E.; and Garnett, R., eds., *Advances in Neural Information Processing Systems 32*, 8024–8035. Curran Associates, Inc.
- Raven, J. C. 1936. Mental tests used in genetic studies: The performance of related individuals on tests mainly educative and mainly reproductive. *Unpublished master’s thesis, University of London*.
- Raven, J. C. 1941. Standardization of progressive matrices, 1938. *British Journal of Medical Psychology*.
- Raven, J. C.; and Court, J. H. 1998. *Raven’s progressive matrices and vocabulary scales*. Oxford psychologists Press Oxford, England.
- Ridgeway, K. 2016. A survey of inductive biases for factorial representation-learning. *arXiv preprint arXiv:1612.05299*.
- Santoro, A.; Raposo, D.; Barrett, D. G.; Malinowski, M.; Pascanu, R.; Battaglia, P.; and Lillicrap, T. 2017. A simple neural network module for relational reasoning. *Advances in Neural Information Processing Systems*, 30.
- Shu, R.; Chen, Y.; Kumar, A.; Ermon, S.; and Poole, B. 2019. Weakly Supervised Disentanglement with Guarantees. In *International Conference on Learning Representations*.
- Sorrenson, P.; Rother, C.; and Köthe, U. 2020. Disentanglement by nonlinear ica with general incompressible-flow networks (gin). *arXiv preprint arXiv:2001.04872*.
- Tschannen, M.; Bachem, O.; and Lucic, M. 2018. Recent advances in autoencoder-based representation learning. *arXiv preprint arXiv:1812.05069*.
- van Steenkiste, S.; Locatello, F.; Schmidhuber, J.; and Bachem, O. 2019. Are Disentangled Representations Helpful for Abstract Visual Reasoning? In *Advances in Neural Information Processing Systems*, 14245–14258.
- Wang, J.; Song, Y.; Leung, T.; Rosenberg, C.; Wang, J.; Philbin, J.; Chen, B.; and Wu, Y. 2014. Learning fine-grained image similarity with deep ranking. In *Proceedings of the IEEE conference on computer vision and pattern recognition*, 1386–1393.
- Wang, K.; and Su, Z. 2015. Automatic generation of raven’s progressive matrices. In *Twenty-Fourth International Joint Conference on Artificial Intelligence*.
- Zhang, C.; Gao, F.; Jia, B.; Zhu, Y.; and Zhu, S.-C. 2019. Raven: A dataset for relational and analogical visual reasoning. In *Proceedings of the IEEE Conference on Computer Vision and Pattern Recognition*, 5317–5327.